Autoclaving-induced in-situ grown alumina on arc-sprayed aluminum coatings: Multiscaled topography facilitates antifouling performances

Xiaoyan He [a,b], Yi Liu [a], Yongfeng Gong [a], Chengxu Zhou [c], Hua Li [a,*]

[a] Key Laboratory of Marine Materials and Related Technologies, Zhejiang Key Laboratory of Marine Materials and Protective Technologies, Ningbo Institute of Materials Technology and Engineering, Chinese Academy of Sciences, Ningbo 315201, China
[b] University of Chinese Academy of Sciences, Beijing 100049, China
[c] School of Marine Sciences, Ningbo University, Ningbo 315211, China

ARTICLE INFO

ABSTRACT

Topographical morphologies of arc sprayed aluminum coatings were tailored by post-spray steam sterilization processing at 120 °C. The porous needle-like nanostructures show the oxide grains of 250 nm in length and 60 nm in width grown on the surface of the coatings. The in-situ growth of the top alumina layer with the unique nano-patterns on aluminum coatings together with the flattened topography of aluminum formed during the spraying gave rise to a unique micro-/nano- hybrid structure. The structure and the presence of alumina synergistically offer the coatings excellent capability to inhibit effectively the adhesion of marine alga *Chlorella* and *Phaeodactylum tricornutum*. Potentiodynamic polarization testing further evidenced significantly enhanced corrosion resistance of the aluminum coatings after the autoclaving treatment. The results would give insights into processing thermal sprayed metallic coatings for desired topological structures for versatile properties.

© 2016 Elsevier B.V. All rights reserved.

1. Introduction

Steel structures such as bridges, wharfs, platforms, and pipeline systems used in the harsh marine environment are susceptible to corrosion and biofouling, causing great loss in economy [1]. A series of measures have been taken to alleviate corrosion, among which thermal spray has become a prominent method to prevent effectively the corrosion due to the advantages of easy operation, low cost and versatile coating materials for long-term applications [2]. Among the thermal sprayed inorganic coatings, aluminum coating is proven efficient for protecting the marine structures against corrosion owing to its low electrode potential for protective anodizing and favorable capability of resisting oxidation [3]. Aluminum coatings have been successfully fabricated by various thermal spray techniques for instance plasma spray [4], arc spray [5], or high velocity oxy-fuel spray [6]. Among these processes, arc spray has been the most competitive method for making aluminum coatings with cost-efficiency and inspiring quality and service life of the coatings [5,7,8]. It was reported that arc spayed aluminum coatings have provided >20 years maintenance-free services in the marine environment [9]. For long-term functional services in the marine environment, post-spray sealing is usually essential for aluminum coatings [9], which yet persists as the major cause of failure of the

coatings. There have been reports claiming that a highly stable, continuous, compact and insoluble passive alumina film formed on the surface of aluminum coating offered protection in both atmospheric and marine circumstances [10]. Development of competitive processing techniques for easy construction of the oxide layer on the top surface of aluminum coatings is therefore of significant importance for enhanced anti-corrosion performances.

As another key concern for the coatings used in the marine environment, biofouling has multiple impacts on corrosion. In the marine environment, it is acknowledged that >20% of the overall corrosion is associated with microbial corrosion and degradation [11,12]. Biocorrosion is usually induced through important changes in the variables like ions, pH values, and oxygen level in localized regions [13,14], since biofilm would acts as a diffusion barrier to prevent the diffusion of either oxygen or aggressive ions [14]. In that case, it is easy to form oxygen concentration cell which leads to crevice or pitting corrosion [15]. Meanwhile, metabolic productions of aggressive compounds such as hydrogen influence corrosion [16] and anodic or cathodic reactions accelerate corrosion by depolarization effect [17]. To control the biocorrosion, it is essential to avoid formation of inhomogeneous biofilm. As one of the major constituents of biofilm, bacteria such as sulfate-reducing bacteria, *pseudomonas aeruginosa* and some algae [17,18] participate in the biocorrosion and bring about great damage. Reducing the adhesion of the species is therefore the most efficient yet simplest approach to alleviate biocorrosion. However, construction of antifouling coatings predominantly pertains to use of polymer-based materials [19,20]. To

* Corresponding author.
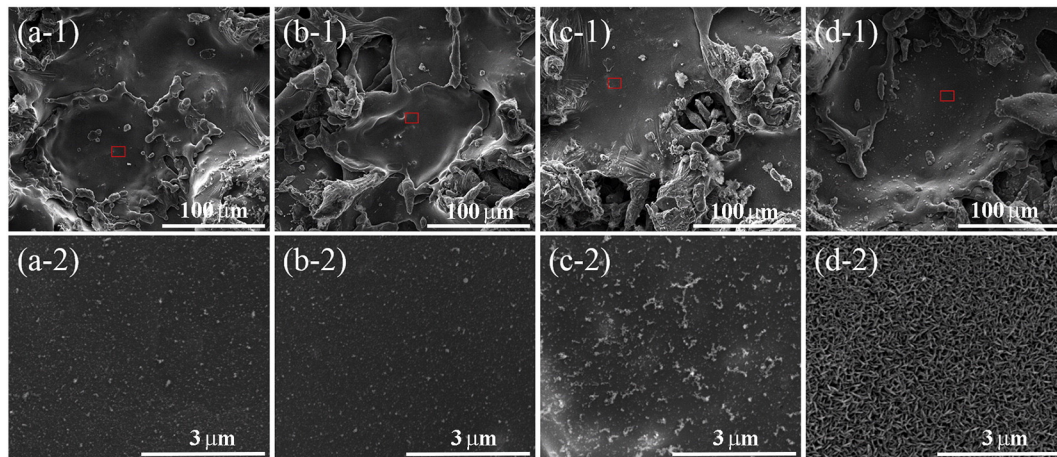 *E-mail address:* lihua@nimte.ac.cn (H. Li).

Fig. 1. Surface morphologies of the as-sprayed coating (a), the post-spray flame-treated coating (b), the post-spray annealed coating (c), and the post-spray autoclaved coating (d) (−2 is high magnification view of the boxed area in −1, respectively).

the best knowledge of the authors, there are no available scientific reports so far focusing on antifouling characteristics of thermal sprayed aluminum coatings.

In this paper, thin alumina layer was produced on arc sprayed aluminum coatings. Three processing routes, namely flame heating, furnace heating, and autoclaving treatment, were employed for oxidation treatment of the top layer of the aluminum coatings after the spraying. All the treatments resulted in formation of thin alumina layer, however, the autoclaving treatment operated at 120 °C gave rise to formation of needle-like patterned nanostructured alumina. Apart from significantly enhanced anti-corrosion performances, the nano-patterned oxides showed exciting antifouling characteristics, as suggested by their
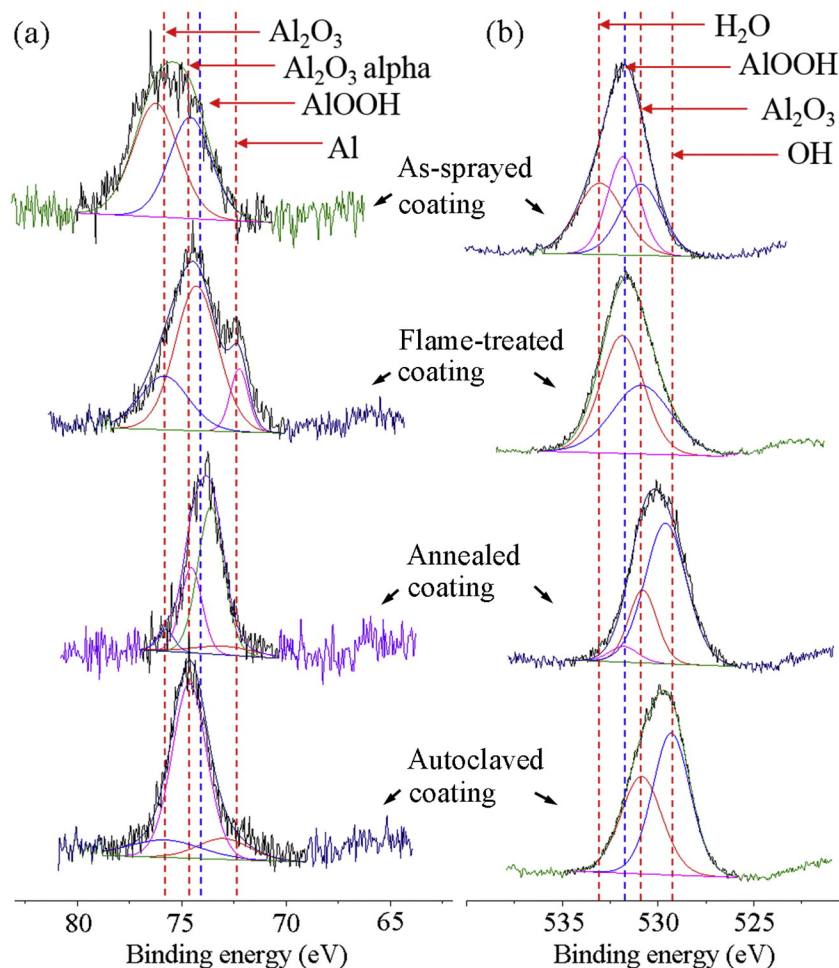

Fig. 2. XPS spectra detected from the surfaces of the coating samples, (a) Al 2p spectra, and (b) O 1s spectra. All spectra were corrected to the polluted C 1s spectra.

Table 1
Content of elements O and Al in the coatings.

Coating sample	O 1s (at.%)	Al 2p (at.%)	Content of O for Al_2O_3 (at.%)
As-sprayed Al coating	64.392	35.608	19.94607
Flame-treated Al coating	61.763	38.763	27.49627
Annealed Al coating	68.823	31.177	17.0447
Autoclaved Al coating	67.971	32.029	29.12693

remarkable capability to resist attachment and colonization of *Chlorella* and *Phaeodactylum tricornutum*. The mechanisms were further discussed and elucidated.

2. Materials and methods

2.1. Fabrication and characterization of the coatings

Aluminum coatings were deposited by high velocity arc spray (AS, TLAS-500C, China). For the spraying, the current and voltage of the arc were set at 80–100 A and 25 V respectively, and the spray distance was 15 cm. The compressed air with a pressure of 0.5 MPa was used for the spraying. The coatings with the thickness of ~150 μm were deposited on 316 L stainless steel substrates of $20 \times 20 \times 2$ mm in dimension. To achieve oxidation of aluminum on the top surface of the coatings, three different technical routes were employed, namely flame heating by a flame spray gun (FS-4 system, Wuhan Research Institute of Materials Protection, China), annealing treatment at 450 °C for 2 h, and 120 °C steam sterilization for 20 min. For optimization purposes, steam treatment at 100 °C for 20 min and 120 °C for 10 min, 40 min, and 60 min was also carried out for the coating samples. The oxidation treatment by flame spray was carried out by scanning the surface of the as-sprayed coatings by the flame gun. Microstructural features of the samples were examined by field emission scanning electron microscopy (FESEM, FEI Quanta FEG 250, the Netherlands). The chemistry of the coatings was further analyzed by X-ray photoelectron spectroscopy (XPS, AXIS Ultra DLD, Kratos).

2.2. Preparation of algal strains and algal adhesion testing

Antifouling performances of the coatings after construction of the top oxide layer were assessed by examining the adhesion of typical marine algae on their surfaces. The adhesion testing was conducted in artificial seawater (ASW) prepared according to ASTM D1141-98. All reagents and solvents were used as received without any further

purification. Marine strains *Chlorella* (Chlorophyta) and *Phaeodactylum tricornutum* (Bacillariophyta) were selected for the testing. The spherically shaped *Chlorella* was categorized as one of the colonizers on artificial surface in the marine environment [21,22]. *Phaeodactylum tricornutum* are coastal marine pennate diatoms that are usually considered as model organism for diatom-related research [23,24], and they participate in the early stage of biofouling and often dominate the fouling [25]. *Chlorella* was cultured in enriched filtered sterilized seawater with Guillard's F/2 growth medium, while *Phaeodactylum tricornutum* was cultured in sterilized seawater with silicate-enriched Guillard's F/2 growth medium. The algae were cultured in an incubator with a 12 h: 12 h light/dark cycle at 22 °C. The algae used in our experiments were in the exponential phase of growth.

4 ml algal suspension with the algal concentration of 5×10^6 ml^{-1} were used for the adhesion testing. The coating samples were soaked by the algal suspension in shaker (to avoid deposition) for 3 days with a 12 h:12 h light/dark cycle at 22 °C. Prior to being put in 6-well plates, the coating samples were ultrasonically washed with ethanol and subsequent deionized water and then dried under a flow of dried air at 37 °C. After the incubation, the wafers were washed with sterile seawater to remove the algae that did not adhere and then fixed by 2.5% glutaraldehyde in ASW for 2 h. The samples were observed by confocal laser scanning microscopy (CLSM, Leica TCS SP5, Germany) equipped with LAS AF Lite software and FESEM. For FESEM observation, dehydration of the samples was made through the critical point drying using 25%, 50%, 75%, 90%, and 100% ethanol solution successively. Due to the rough nature of the coating surface, CLSM pictures were captured layer by layer and then were 3D projected by LAS AF Lite software to reconstruct desired images. Adhesion of the algae was in accordance with the content of chlorophyll *a*. Chlorophyll a in ethanol solvent was detected at the wavelength of 629 nm, 649 nm, and 665 nm by a microplate reader (SpectraMax 190, Molecular Devices, USA) following a previously established protocol [26]. The equation for calculating chlorophyll *a* (Chl a) of *Chlorella* in ethanol was: Chl a (μg/ml) $\approx -5.2007A_{649} + 13.5275A_{665}$ and that of *Phaeodactylum tricornutum* was: Chl a (μg/ml) $\approx -1.4014A_{629} + 12.1551A_{665}$ as per the reported protocol [26]. Each testing was repeated in triplicate.

2.3. Potentiodynamic polarization testing

Prior to the testing, the coating samples were sealed by epoxy with an exposed testing surface area of 10×10 mm^2. A traditional three-electrode cell was used, with 1 cm^2 platinum as the counter electrode, a saturated calomel electrode (SCE) as the reference electrode and the specimen as the working electrode. Polarization curves were acquired
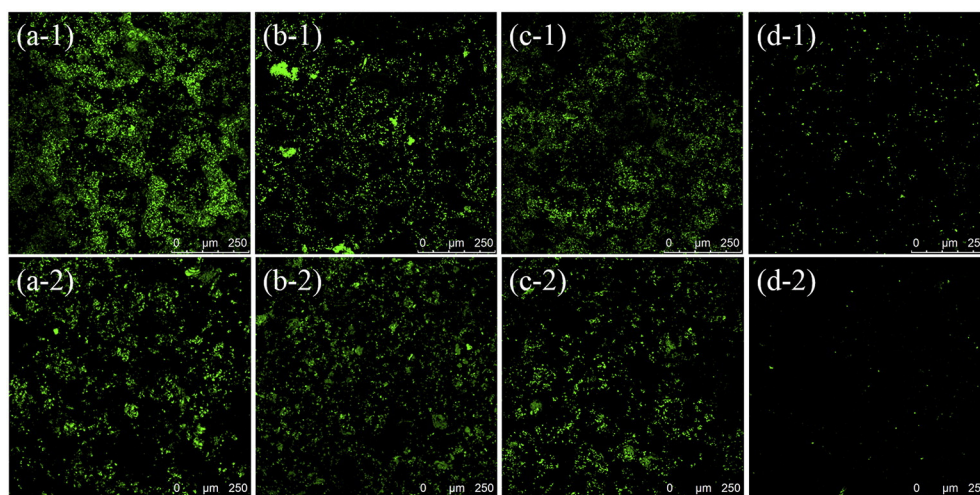

Fig. 3. CLSM images showing adhesion of *Chlorella* (−1) and *Phaeodactylum tricornutum* (−2) on the as-sprayed Al coating (a), the post-spray flame-treated Al coating (b), the post-spray annealed Al coating (c), and the post-spray autoclaved Al coating (d).
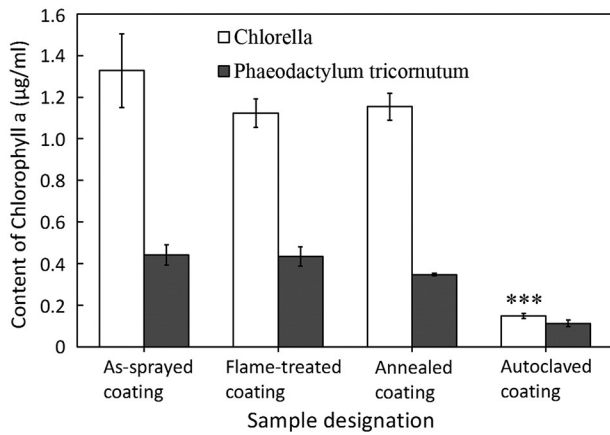
Fig. 4. Content of chlorophyll *a* detected from the adhered *Chlorella* and *Phaeodactylum tricornutum* on the coatings. Error bars are shown as $\pm$SD (n = 3). ***: p < 0.005 as compared with the as-sprayed coating. The testing was conducted after 3 days incubation of the coating samples.

on a Solartron Modulab system (2100A, UK) for the samples immersed in room temperature ASW without stirring. Potentiodynamic polarization curves were acquired with the potential range of −500 mV to 500 mV versus E_{ocp} at a scan rate of 0.5 mV/s and the corrosion potential (E_{corr}) and the corrosion current density (I_{corr}) were calculated by Modulab software. Each testing was repeated in triplicate.

3. Results and discussion

The as-sprayed aluminum coating exhibits a typical laminar structure and flattened aluminum splats are clearly seen on their surfaces (Fig. 1a). Complete melting state of aluminum is suggested. Close view of the surface of the as-sprayed coating shows appearance of many irregular particles with granular sizes <100 nm (mean granular size: ~20 nm, Fig. 1a-1). This structural feature is also observed on the surfaces of the flame treated coating (Fig. 1b) and the annealed coating (Fig. 1c). Aggregation of the irregular particles is shown for the annealed coating (Fig. 1c-2 versus a-2 and b-2), exhibiting enlarged granular sizes of up to 600 nm. Surprisingly, however, it is noted that the autoclaving treatment at 120 °C for 20 min brought about distinctive topographical features, that is, needle-like grains with unique patterns are seen on the surface of the coating (Fig. 1d). Other autoclaving treatment conditions did not bring about formation of the nanostructures. The patterned structure shows the grains of ~250 nm in length and ~60 nm in width. This is indeed a multiscaled micro−/nano- structure (Fig. 1d-1 and d-2).

Further XPS detection indicates occurring of oxidation of aluminum during either the coating fabrication stage or the post-spray treatments (Fig. 2), regardless of the fact that the oxidation extent differs in the top layer of the coatings. For the XPS analyses, carbon peak was used as an internal calibration standard. Al 2p spectrum is acquired and the envelopes are respectively fitted with more than two components, without the spin-orbit splitting of Al 2p level, although the separations of the Al 2p spectra from aluminum oxides or hydroxides are <1 eV [27]. The irregular grains (Fig. 1a-2, b-2, c-2) and the needle-like grains (Fig. 1d-2) are alumina phase. The broad nature of the Al 2p peak indicates that the surface components of the as-sprayed aluminum coating consists of halides (76.58 eV) and Al_2O_3 alpha (74.58 eV) [28]. The appearance of a shoulder on the low-binding-energy side of the flame-treated coating is attributed to Al phase, which also consists of alumina at 75.8 eV [29] and AlOOH at 74.26 eV [30]. The XPS curve for the annealed coating also shows presence of the peaks for Al, AlOOH (73.64 eV), alpha-Al_2O_3 and Al_2O_3. Alumina is the dominate phase in the thin top layer of the autoclaving treated aluminum coating. Additional XPS detection for oxygen suggests the same results (Fig. 2b). O1s peak is smooth and broad, and is located in the range of 529.60–531.80 eV with a full-width at half maxima of around 3 eV. It appears that the oxygen signal is mainly attributed to AlOOH (531.80 eV) [31], Al_2O_3 (530.80 eV) [32], OH (529.60 eV) [33], and H_2O (532.93 eV) [32]. Surprisingly, trace of AlOOH is detected on the O1s curve, but it was not observed on Al2p spectra. It is therefore speculated that AlOOH is not stable, and easily forms Al_2O_3 by the decomposition: $2AlOOH\ (s) = Al_2O_3\ (s) + H_2O\ (g)$ [29].

Aluminum has high reactivity toward water and oxygen [30], and this could easily explain the appearance of alumina on the as-sprayed aluminum coating. The XPS results suggest alternative extents of the oxidation of aluminum on the surfaces of the coatings, and the newly in-situ grown layer with the needle-like structure comprises alumina. For the as-sprayed coating, the flame treated coating, and the annealing treated coating, aluminum reacts directly with oxygen in air to form alumina. It is not surprising that more alumina was seen for the flame-heated coatings than the as-sprayed one (Table 1) since further oxidation is anticipated during the heating. In the autoclaving environment, aluminum likely reacts with water steam through the following reaction: $2Al\ (s) + 3H_2O\ (g) = Al_2O_3\ (s) + 3H_2\ (g)$ [34]. Formation of the needle-like alumina grains is attributed to the particular treating conditions, 120 °C steam sterilization for 20 min. Surface roughing of aluminum alloy is usually accomplished by boiling water treatment [35,36] through the chemical reaction of Al with H_2O and physical erosion of air bubble [34]. In our case, it is speculated that gas escaping could be mainly responsible for the formation of the patterned nanostructures of the grown alumina since $H_2\ (g)$ could easily get out without water barrier. Taking into account the pre-existing micron-sized
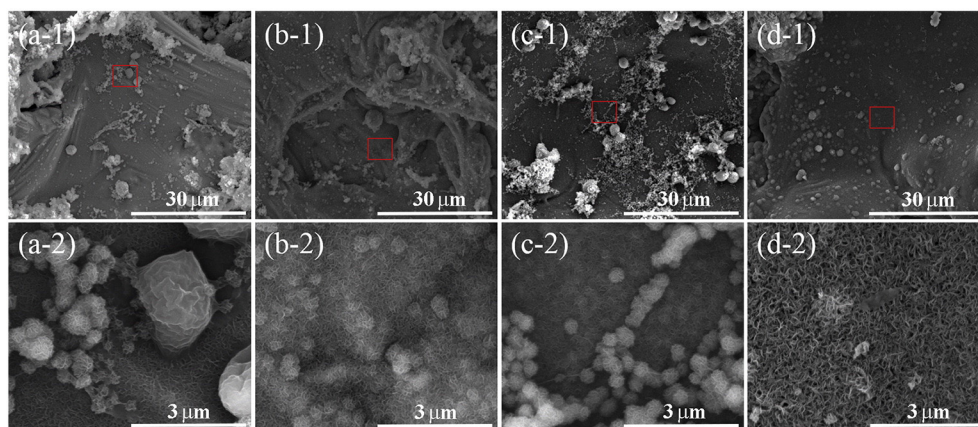

Fig. 5. SEM images showing the topographical morphology of the coatings after 3 days incubation in *Chlorella*-containing solution, (a) the as-sprayed coating, (b) the post-spray flame-treated coating, (c) the post-spray annealed coating, and (d) the post-spray autoclaved coating (−2 is high magnification view of the boxed area in −1, respectively).

Fig. 6. SEM images showing the topographical morphology of the coatings after 3 days incubation in *Phaeodactylum tricornutum*-containing solution, (a) the as-sprayed coating, (b) the post-spray flame-treated coating, (c) the post-spray annealed coating, and (d) the post-spray autoclaved coating (−2 is high magnification view of the boxed area in −1, respectively).
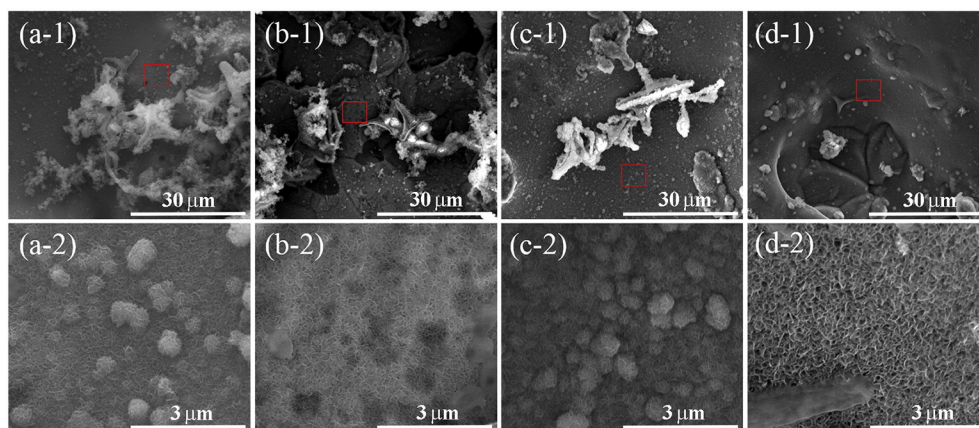
surface roughness of the as-sprayed aluminum coating, the autoclaved coating already possesses micro-/nano- hybrid topography, which would in turn facilitate multiple functions of the coatings. Among the performances expected for aluminum coatings used in the marine environment, anti-corrosion is the predominate concern, which has been extensively investigated and elucidated [35]. The special structural features exhibited by the autoclaving treated aluminum coatings might offer the coatings antifouling function, which has never been realized for aluminum coatings.

The antifouling testing against adhesion of algae indeed suggests excellent antifouling performances of the autoclaving treated coatings. CLSM observation of the aluminum coatings after incubation in the media containing *Chlorella* and *Phaeodactylum tricornutum* for 3 days shows that the micro-/nano- surface pattern gave rise to effectively constrained colonization of the species (Fig. 3). This is encouraging since it is the first time to note such antifouling properties of thermal sprayed aluminum coatings. However, the presence of alumina phases alone does not provide the coatings with the antifouling characteristics (Fig. 3b, c). Multiple layers of the algae and even their aggregation are seen for the as-sprayed coating, the flame-heated coating, and the annealed coating (Fig. 3a, b, c), even though slight differences in adhered diatoms are evident for the samples. Adhesion of *Phaeodactylum tricornutum* and *Chlorella* is hardly seen on the surface of the autoclaved aluminum coating, evidencing the promising effect achieved by the in-situ formed micro-/nano- hybrid surface structures.

Adhesion of the algae on the coatings was further quantitatively assessed by calculating chlorophyll *a* (Fig. 4), which is directly related to the number of adhered algae. Slight difference in adhered *Chlorella* is revealed for the as-sprayed coating, the flame-treated coating, and the annealed coating, whereas the attachment and colonization of

Chlorella on the autoclaved coating is significantly constrained (0.15 μg/ml versus 1.33 μg/ml, 1.12 μg/ml, and 1.15 μg/ml). Similar trend is also realized for the adhesion of *Phaeodactylum tricornutum* (0.11 μg/ml versus 0.44 μg/ml, 0.43 μg/ml, and 0.35 μg/ml). In addition, content of chlorophyll *a* from *Chlorella* differs from the other species, *Phaeodactylum tricornutum*. There is therefore no doubt that the textured alumina layer reduced algal adhesion.

Morphological examination by FESEM of the samples after the incubation in the algae-containing solution shows adhered *Chlorella* and *Phaeodactylum tricornutum* on the as-sprayed coating, the flame-treated coating, and the annealed coating (Figs. 5, 6). For these coating samples, Al_2O_3 particles are seen on their surfaces, which is most likely due to galvanic corrosion of aluminum in the solution. This did not happen for the autoclaved coatings (Figs. 5d and 6d). It is interesting to note that after the incubation, all the coatings show needle-like surface morphology. However, the physical features, e.g., shape and size, of the grains are markedly different from those of the needle-like alumina induced by the autoclaving treatment. The structure on those three types of coatings is apparently formed by the corrosion products after the immersion in algal suspensions [1]. The autoclaved coating shows negligible changes in topographical morphology, that is, the alumina nano-pattern keeps almost intact even after the 3 days incubation. This phenomenon on the other hand indicates that the in-situ grown Al_2O_3 isolates direct contact of aluminum coating with ASW, in turn achieving enhanced corrosion resistance.

The enhanced corrosion resistance is evidenced by the electrochemical testing (Fig. 7). The potentiodynamic polarization curves show clearly significantly reduced corrosion current and slightly increased corrosion voltage, suggesting decreased corrosion rate and reinforced capability to resist corrosion. E_{corr} of the as-sprayed coating, the flame-treated coating, the annealed coating, and the autoclaving-treated coating is −761.5 mV, −794.7 mV, −786.7 mV, and −768.4 mV, respectively. Appearance of the breakdown of potential above about −250 mV for the autoclaved coating likely indicates micro-cracking of the passive film on its surface. Significant changes in I_{corr} and corrosion rate for the coatings are also obtained. Significantly decreased corrosion density is revealed for the autoclaving treated coating (1.44 μA/cm^2) as compared to the as-sprayed coating (19.09 μA/cm^2), the flame treated coating (2.26 μA/cm^2), and the annealed coating (19.48 μA/cm^2). It was reported that ASW facilitates galvanic corrosion by contact between different metals such as 316 L and aluminum coating [4] and triggers formation of a galvanic cell to accelerate aluminum coating corrosion [37].

Since thermal sprayed aluminum coating is usually porous in nature, in order to improve its corrosion resistance, sealing or other surface modification is essential. Our research proves that surface oxidation alone does not provide the coating with altered anti-corrosion or
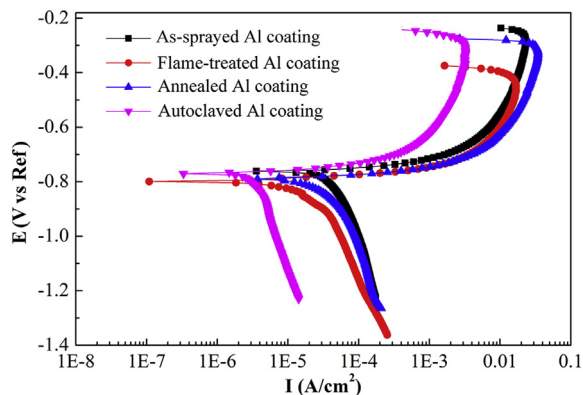

Fig. 7. Potentiodynamic polarization curves of the coatings.

antifouling performances. Instead, it is exciting to note that oxidation of the top thin layer of the aluminum coating and the textured topography synergistically affect the performances. The arc spray alone already equips the coating with micron-sized rough surface, and the additional oxidation treatment in autoclaving environment further gives the coating nanosized texture. The most striking finding of this research is that the multiscaled oxide structure exhibits remarkable antifouling performances. The individual alga is likely bridged by several adjacent oxide grains upon its settlement since its size is much larger than individual oxide grains. Significantly decreased attachment area would reduce the adhesion [38]. In addition, the newly grown Al_2O_3 layer with very little conductivity [10] on aluminum coating can also serve as dielectric shielding confining electrical charge transport and ions exchange to the corrodible area, thereby improving the corrosion resistance of the coating. The autoclaving approach shows great promise for constructing nano-porous alumina grains on thermal sprayed aluminum coatings for their widespread marine applications.

4. Conclusions

Steam sterilization treatment at 120 °C has been carried out for arc sprayed aluminum coatings and newly grown alumina was accomplished on their surfaces. The layer comprising needle-like alumina grains possesses nano-porous topographical structure. The micro-/nano- hybrid structural feature and the alumina phase synergistically play roles in enhancing the anti-corrosion and antifouling performances. It is for the first time realized that the unique topographical pattern resists effectively adhesion of typical marine algae. In addition, formation of the continuous, adhesive, insoluble and strongly passive alumina film provides the aluminum coating with an excellent barrier and protective layer against corrosion. The results would give insight into in-situ construction of inert oxide layer with patterned topography on metallic coatings for extensive applications.

Acknowledgements

References

[1] J. Duan, S. Wu, X. Zhang, G. Huang, M. Du, B. Hou, Corrosion of carbon steel influenced by anaerobic biofilm in natural seawater, Electrochim. Acta 54 (2008) 22–28.
[2] S.J. Kim, S.K. Jang, S.J. Lee, Observation of damage behavior with spray distance for Al-Zn-Zr thermal spray coating, Surf. Interface Anal. 44 (2012) 1393–1396.
[3] F. Ahnia, B. Demri, Evaluation of aluminum coatings in simulated marine environment, Surf. Coat. Technol. 220 (2013) 232–236.
[4] F. Vargas, H. Ageorges, P. Fauchais, M.E. Lopez, J.A. Calderon, Permeation of saline solution in Al_2O_3-13 wt.% TiO_2 coatings elaborated by atmospheric plasma spraying, Surf. Coat. Technol. 220 (2013) 85–89.
[5] J.H. Kim, M.H. Lee, A study on cavitation erosion and corrosion behavior of Al-, Zn-, Cu-, and Fe-based coatings prepared by arc spraying, J. Therm. Spray Technol. 19 (2010) 1224–1230.
[6] R.J.K. Wood, A.J. Speyer, Erosion-corrosion of candidate HVOF aluminium-based marine coatings, Wear 256 (2004) 545–556.
[7] J. Huang, Y. Liu, J. Yuan, H. Li, Al/Al_2O_3 composite coating deposited by flame spraying for marine applications: alumina skeleton enhances anti-corrosion and wear performances, J. Therm. Spray Technol. 23 (2014) 676–683.
[8] S. Kuroda, J. Kawakita, M. Takemoto, An 18-year exposure test of thermal-sprayed Zn, Al, and Zn-Al coatings in marine environment, Corrosion 62 (2006) 635–647.
[9] F.S. Rogers, Thermal spray for commercial shipbuilding, J. Therm. Spray Technol. 6 (1997) 291–293.
[10] O. de Rincon, A. Rincon, M. Sanchez, N. Romero, O. Salas, R. Delgado, B. Lopez, J. Uruchurtu, M. Marroco, Z. Panosian, Evaluating Zn, Al and Al-Zn coatings on carbon steel in a special atmosphere, Constr. Build. Mater. 23 (2009) 1465–1471.
[11] S.J. Yuan, S.O. Pehkonen, Y.P. Ting, K.G. Neoh, E.T. Kang, Antibacterial inorganic-organic hybrid coatings on stainless steel via consecutive surface-initiated atom transfer radical polymerization for biocorrosion prevention, Langmuir 26 (2010) 6728–6736.
[12] S.J. Yuan, F.J. Xu, S.O. Pehkonen, Y.P. Ting, K.G. Neoh, E.T. Kang, Grafting of antibacterial polymers on stainless steel via surface-initiated atom transfer radical polymerization for inhibiting biocorrosion by *Desulfovibrio desulfuricans*, Biotechnol. Bioeng. 103 (2009) 268–281.
[13] H.A. Videla, Prevention and control of biocorrosion, Int. Biodeterior. Biodegrad. 49 (2002) 259–270.
[14] H.A. Videla, L.K. Herrera, Microbiologically influenced corrosion: looking to the future, Int. Microbiol. 8 (2005) 169–180.
[15] T.S. Rao, A.J. Kora, P. Chandramohan, B.S. Panigrahi, S.V. Narasimhan, Biofouling and microbial corrosion problem in the thermo-fluid heat exchanger and cooling water system of a nuclear test reactor, Biofouling 25 (2009) 581–591.
[16] A. Heyer, F. D'Souza, C.F.L. Morales, G. Ferrari, J.M.C. Mol, J.H.W. de Wit, Ship ballast tanks a review from microbial corrosion and electrochemical point of view, Ocean Eng. 70 (2013) 188–200.
[17] H. Videla, Biocorrosion and biofouling of metals and alloys of industrial usage. Present state of the art at the beginning of the new millennium, Rev. Metal. Madrid 32 (2003) 245–253.
[18] N. Labjar, M. Lebrini, F. Bentiss, N.E. Chihib, S. El Hajjaji, C. Jama, Corrosion inhibition of carbon steel and antibacterial properties of aminotris-(methylenephosphonic) acid, Mater. Chem. Phys. 119 (2010) 330–336.
[19] C.F. Ma, H.J. Yang, X. Zhou, B. Wu, G.Z. Zhang, Polymeric material for anti-biofouling, Colloids Surf. B. Biointerfaces 100 (2012) 31–35.
[20] C.F. Ma, L.G. Xu, W.T. Xu, G.Z. Zhang, Degradable polyurethane for marine anti-biofouling, J. Mater. Chem. B 1 (2013) 3099–3106.
[21] S. Ma, Q. Ye, X. Pei, D. Wang, F. Zhou, Antifouling on Gecko's feet inspired fibrillar surfaces: evolving from land to marine and from liquid repellency to algae resistance, Adv. Mater. Interfaces 2 (2015) 1500257.
[22] F. Wan, Q. Ye, B. Yu, X.W. Pei, F. Zhou, Multiscale hairy surfaces for nearly perfect marine antibiofouling, J. Mater. Chem. B 1 (2013) 3599–3606.
[23] J. Landoulsi, K.E. Cooksey, V. Dupres, Review-interactions between diatoms and stainless steel: focus on biofouling and biocorrosion, Biofouling 27 (2011) 1105–1124.
[24] K.C. Anyaogu, A.V. Fedorov, D.C. Neckers, Synthesis, characterization, and antifouling potential of functionalized copper nanoparticles, Langmuir 24 (2008) 4340–4346.
[25] N. Poulsen, N. Kroeger, M.J. Harrington, E. Brunner, S. Paasch, M.T. Buhmann, Isolation and biochemical characterization of underwater adhesives from diatoms, Biofouling 30 (2014) 513–523.
[26] R.J. Ritchie, Consistent sets of spectrophotometric chlorophyll equations for acetone, methanol and ethanol solvents, Photosynth. Res. 89 (2006) 27–41.
[27] H. Liao, R. Sodhi, T.W. Coyle, Surface composition of AlN powders studied by x-ray photoelectron spectroscopy and bremsstrahlung-excited Auger electron spectroscopy, J. Vac. Sci. Technol. A 11 (1993) 2681–2686.
[28] O. Böse, E. Kemnitz, A. Lippitz, W. Unger, C 1s and Au 4f7/2 referenced XPS binding energy data obtained with different aluminium oxides,-hydroxides and-fluorides, Fresenius J. Anal. Chem. 358 (1997) 175–179.
[29] A. Nylund, I. Olefjord, Surface analysis of oxidized aluminium. 1. Hydration of Al_2O_3 and decomposition of $Al(OH)_3$ in a vacuum as studied by ESCA, Surf. Interface Anal. 21 (1994) 283–289.
[30] S. Thomas, P.M. Sherwood, Valence band spectra of aluminum oxides, hydroxides, and oxyhydroxides interpreted by X. alpha. calculations, Anal. Chem. 64 (1992) 2488–2495.
[31] T.L. Barr, An ESCA study of the termination of the passivation of elemental metals, J. Phys. Chem. 82 (1978) 1801–1810.
[32] S. Briggs, D. Practical surface analysis, Auger- and X-ray Photoelectron Spectroscopy, 1, Wiley, Cichester, 1990.
[33] S. Maroie, G. Haemers, J. Verbist, Surface oxidation of polycrystalline α (75% Cu/25% Zn) and β (53% Cu/47% Zn) brass as studied by XPS: influence of oxygen pressure, Appl. Surf. Sci. 17 (1984) 463–467.
[34] S. Ren, S. Yang, Y. Zhao, T. Yu, X. Xiao, Preparation and characterization of an ultrahydrophobic surface based on a stearic acid self-assembled monolayer over polyethyleneimine thin films, Surf. Sci. 546 (2003) 64–74.
[35] L. Feng, H. Zhang, Z. Wang, Y. Liu, Superhydrophobic aluminum alloy surface: fabrication, structure, and corrosion resistance, Colloids Surf. A Physicochem. Eng. Asp. 441 (2014) 319–325.
[36] L. Feng, H. Li, Y. Song, Y. Wang, Formation process of a strong water-repellent alumina surface by the sol-gel method, Appl. Surf. Sci. 256 (2010) 3191–3196.
[37] J. Kawakita, S. Kuroda, T. Kodama, Evaluation of through-porosity of HVOF sprayed coating, Surf. Coat. Technol. 166 (2003) 17–23.
[38] J. Xu, W. Zhao, S. Peng, Z. Zeng, X. Zhang, X. Wu, Q. Xue, Investigation of the biofouling properties of several algae on different textured chemical modified silicone surfaces, Appl. Surf. Sci. 311 (2014) 703–708.